A&A 395, 573–585 (2002)
DOI: 10.1051/0004-6361:20021334

Astronomy & Astrophysics

Water emission in NGC 1333–IRAS 4⋆

The physical structure of the envelope

S. Maret[1], C. Ceccarelli[2,3], E. Caux[1], A. G. G. M. Tielens[4], and A. Castets[2]

[1] Centre d'Étude Spatiale des Rayonnements, CESR/CNRS-UPS, BP 4346, 31028 Toulouse Cedex 04, France
[2] Observatoire de Bordeaux, BP 89, 33270 Floirac, France
[3] Laboratoire d'Astrophysique, Observatoire de Grenoble, BP 53, 38041 Grenoble Cedex 09, France
[4] Space Research Organization of the Netherlands, PO Box 800, 9700 AV Groningen, The Netherlands

Received 27 May 2002 / Accepted 5 September 2002

Abstract. We report ISO-LWS far infrared observations of CO, water and oxygen lines towards the protobinary system IRAS 4 in the NGC 1333 cloud. We detected several water, OH, CO rotational lines, and two [OI] and [CII] fine structure lines. Given the relatively poor spectral and spatial resolution of these observations, assessing the origin of the observed emission is not straightforward. In this paper, we focus on the water line emission and explore the hypothesis that it originates in the envelopes that surround the two protostars, IRAS 4 A and B, thanks to an accurate model. The model reproduces quite well the observed water line fluxes, predicting a density profile, mass accretion rate, central mass, and water abundance profile in agreement with previous works. We hence conclude that the emission from the envelopes is a viable explanation for the observed water emission, although we cannot totally rule out the alternative that the observed water emission originates in the outflow. The envelopes are formed by a static envelope where the density follows the r^{-2} law, at $r \geq 1500$ AU, and a collapsing envelope where the density follows the $r^{-3/2}$ law. The density of the envelopes at 1500 AU from the center is $\sim 4 \times 10^6$ cm^{-3} and the dust temperature is ∼30 K, i.e. about the evaporation temperature of CO-rich ices. This may explain previous observations that claimed a factor of 10 depletion of CO in IRAS 4, as those observations probe the outer ≤30 K region of the envelope. The water is $\sim 5 \times 10^{-7}$ less abundant than H_2 in the outer and cold envelope, whereas its abundance jumps to $\sim 5 \times 10^{-6}$ in the innermost warm region, at $r \leq 80$ AU where the dust temperature exceeds 100 K, the evaporation temperature of H_2O-rich ices. We derive a mass of 0.5 $M_\odot$ for each protostar, and an accretion rate of 5×10^{-5} $M_\odot$ yr^{-1}, implying an age of about 10000 years, if the accretion rate remains constant. We finally discuss the difference between IRAS 4 and IRAS 16293-2422, where a similar analysis has been carried out. We found that IRAS 4 is probably a younger system than IRAS 16293-2422. This fact, coupled with the larger distance of IRAS 4 from the Sun, fully explains the apparent difference in the molecular emission of these two sources, which is much richer in IRAS 16293-2422.

Key words. stars: formation – stars: circumstellar matter – ISM: molecules – ISM: abundances – stars: individual: NGC 1333-IRAS 4

1. Introduction

The south part of the NGC 1333 reflection nebulae, in the Perseus cloud, is an active star forming region, containing many infrared sources associated with molecular flows and numerous Herbig-Haro objects. IRAS 4 was first identified by Jennings et al. (1987), and further observations (Sandell et al. 1991) revealed IRAS 4 it was a binary system resolved into two components, named IRAS 4A and IRAS 4B, and separated by 31″. Interferometric observations (Lay et al. 1995; Looney et al. 2000) have shown further multiplicity of the two sources. IRAS 4A is itself a binary system with a separation of 10″, and there is some evidences that IRAS 4B could also be a multiple system, with a separation of 0.5″.

The distance of the NGC 1333 cloud is much debated. Herbig & Jones (1983) found a distance of 350 pc for the Perseus OB2 association (a more recent estimate based on the Hipparcos data gives 318 ± 27; de Zeeuw et al. 1999), but extinction observations towards NGC1333 itself (Cernis 1990) suggest that it may be as close as 220 pc. Assuming a distance of 350 pc, Sandell et al. (1991) measured a system total luminosity of 28 $L_\odot$ (11 $L_\odot$ at 220 pc) equally shared between IRAS 4A and B. They derived an envelope mass of 9 and 4 $M_\odot$ respectively (3.5 and 1.5 $M_\odot$ at 220 pc). This relatively large mass, together with the low bolometric luminosity suggest that both sources are deeply embedded and probably very young. They have been classified as *Class 0* sources (Andre et al. 1993). IRAS 4A and B are both associated with molecular outflows, detected in CO, CS (Blake et al. 1995) and

Send offprint requests to: S. Maret,
e-mail: sebastien.maret@cesr.fr

⋆ Based on observations with ISO, an ESA project with instruments funded by ESA Member States (especially the PI countries: France, Germany, The Netherlands and the United Kingdom) with the participation of ISAS and NASA.

SiO (Lefloch et al. 1998) millimeter transitions. The outflow originating from IRAS 4A is very highly collimated, whereas that originating from IRAS 4B is rather compact and unresolved in single dish observations (Knee & Sandell 2000). The dynamical ages of both outflows are a few thousands years.

In the past years, many observational studies have been focused on the continuum emission of IRAS 4. Recent works include maps of the region obtained with IRAM at 1.3 mm (Lefloch et al. 1998) and with SCUBA at 450 and 850 μm (Sandell & Knee 2001). An accurate modeling of the continuum emission has been very recently carried out by Jørgensen et al. (hereafter JSD02, 2002), who reconstructed the dust temperature and density profiles across the two envelopes.

The molecular line emission is probably a better and certainly a complementary tool to probe the dynamical, chemical and physical structure of the envelopes of IRAS 4. The last decade has seen flourishing several studies of molecular line profiles (e.g. Gregersen et al. 1997; Evans 1999) and line spectra (Blake et al. 1995), all having in common the goal of reconstructing the physical structure of the protostellar envelopes. Specifically, Blake et al. (1995) carried out a multifrequency study of several molecules in IRAS 4, including H_2CO and CH_3OH. Their two major results regarding the structure of the IRAS 4 envelopes are: 1) a large depletion, around a factor 10–20, of CO and all molecules in the envelope, and 2) the presence of a region with an increased abundance of CS, SiO and CH_3OH, that the authors attribute to mantles desorption caused by grain-grain collisions induced by the outflows originating from the two protostars. More recently interferometric observations by Di Francesco et al. (2001, see also, Choi et al. 1999) detected an inverse P-cygni profile of the H_2CO $3_{2,1}-2_{1,1}$ line on a $2''$ scale towards both IRAS 4A and B, providing the least ambiguous evidence of infall motion towards a protostar ever. From a simple two-layer modeling, they derived an accretion rate of 1.1×10^{-4} and 3.7×10^{-5} $M_\odot$ yr^{-1}, an inner mass of 0.7 and 0.2 $M_\odot$, and an age of 6500 and 6200 yr (assuming constant accretion rate) for IRAS 4A and IRAS 4B respectively.

In this paper we concentrate on the far infrared (FIR) line spectrum, and in particular the water line spectrum observed with the *Long Wavelength Spectrometer* (Clegg et al. 1996, herein after LWS) on board ISO (Kessler et al. 1996) in the direction of IRAS 4. The goal of this study is to check whether the observed water line emission can be attributed to the thermal emission of the envelopes surrounding the IRAS 4 protobinary system. Water lines have in fact been predicted to be a major coolant of the gas in the collapsing envelopes of low-mass protostars (Ceccarelli et al. 1996, hereafter CHT96; Doty & Neufeld 1997). Given the relatively large range of level energies (from ~100 to ~500 K) and spontaneous emission coefficients (from 10^{-2} to ~1 s^{-1}) of the water transitions observed by ISO-LWS, the observed lines can in particular probe the innermost regions of the envelope. This makes the analysis of the ISO-LWS water lines a precious and almost unique tool (when considering the water abundance across the envelope). The reverse of the coin is that assessing the actual origin of the water emission is somewhat difficult and still debated, as the spectral and spatial resolutions of ISO-LWS are relatively poor to disentangle the various components falling into the beam. For example, strong molecular line emission is often associated with the outflows emanating from young protostars (e.g. Bachiller & Perez Gutierrez 1997). As already mentioned, the line emission from CO, CS and other molecules are certainly contaminated by the outflowing gas in IRAS 4. Nonetheless, low lying lines seem to be more affected than high lying lines in first instance, and different molecules suffer differently from this "contamination", as proved by the Di Francesco et al. (2001) observations. Although water has been predicted to be very abundant in shocked gas, the published ISO observations show that the water emission is usually stronger towards the central sources and weaker, if detected at all, in the direction of the peaks of the outflows powered by low mass protostars (see Ceccarelli et al. 2000a, for a review). When water lines are detected in clear-cut shocked regions, the water abundance seems to be lower than that predicted by the models, like in the case of HH54 (Liseau et al. 1996) or HH7-11 (Molinari et al. 1999; Molinari et al. 2000), or in the outflows of IRAS 4 (see next section). Finally, SWAS observations seem to support the evidence that the water abundance in the shocked regions is a few times 10^{-6} (Neufeld et al. 2000). These facts, together with the apparent correlation between the observed water emission and the 1.3 mm continuum, and the lack of correlation with SiO emission[1] in low mass protostars (Ceccarelli et al. 1999) play in favor of a relatively low contamination of the ISO-LWS observed water emission by the outflow and encourage us to explore in detail this hypothesis for the IRAS 4.

In the specific case of IRAS 4, the *Submillimiter Wavelengths Astronomical Satellite* (SWAS; Melnick et al. 2000) observed the ground o-H_2O line at 557 GHz (Neufeld et al. 2000; Bergin et al. 2002). Given its relatively large linewidth (~18 km s^{-1}) the 557 GHz line is certainly dominated by the outflow emission. Nonetheless, this does not imply that the ISO FIR water lines also originate in the outflow, and this for two reasons. First, the beamwidth (~4′) of the SWAS observations, being about 3 times that of ISO-LWS, encompasses the entire outflow, whereas the ISO observations do not encompass the two emission peaks of the outflow (see also 3.1), but only the envelope. Second, the 557 GHz transition, being the water ground transition, is more easily excited than the FIR water lines, and therefore the latter probably probe different regions. In fact, Bergin et al. (2002) find that most of the 557 GHz line must originate in a component colder, hence different, by that probed by the FIR water lines, even under the assumption that they probe the outflow. To summarize, decicing whether the observed FIR water emission in IRAS 4 originates in the outflow or in the envelope remains an open question, based on the available present observations. In this article we explore in detail the latter hypothesis and submit it to the scrutiny of an accurate modeling, trying hence to answer to the question on a theoretical basis. At this scope we used the CHT96 model, already successfully applied to the solar type protostar IRAS 16293-2422 which allowed to explain more than two dozen observed ISO-LWS water lines and ground-based millimeter SiO and H_2CO

[1] SiO emission is usually associated with the outflow strong shocks (e.g. Bachiller & Perez Gutierrez 1997), and it is believed to be a product of grain mantle desorption (Caselli et al. 1997; Schilke et al. 1997).

lines (Ceccarelli et al. 2000a; Ceccarelli et al. 2000b). One of the major results of that work is the prediction of the existence of a hot core like region in the innermost part of the envelope of IRAS 16293-2422, in which the dust temperature exceeds the evaporation temperature of interstellar ice ($\simeq$100 K). These studies have been confirmed by the recent analysis by Schöier et al. (2002) of several other molecular transitions. Such hot cores are well studied around massive protostars where – driven by reactions among the evaporated ice molecules in the warm gas – their chemical composition differs substantially from that of quiescent clouds (Walmsley 1989; Charnley et al. 1992). Hot cores around low mass protostars may actually have a different chemical composition (Ceccarelli et al. 2000b). This molecular complexity may be of prime interest on account of a possible link to the chemical history of the solar nebula and hence the molecular inventory available to the forming Earth and other solar system planets and satellites.

In order to understand the physical and chemical processes that take place during the first stages of star formation, it would be necessary to undertake a work similar to that the one done on IRAS 16293-2422 on a larger sample of protostars. In this paper we present a study of the structure of the envelope of NGC 1333–IRAS 4, obtained using ISO-LWS observations of the H_2O far-infrared lines. A preliminary analysis of the same set of data has already been presented in Ceccarelli et al. (1999) and Caux et al. (1999a). Here we revisit the data using a new calibration and compare the observations with the CHT96 model predictions, testing a large range of model parameters. This study is part of a large project aimed to model the water emission in several low mass protostars. The water observations are complemented with formaldehyde and methanol ground based observations, to have a complete budget of the most abundant molecules in the innermost regions of the protostellar envelopes (Maret et al. in preparation). Finally, the structure obtained by the analysis of these observations will be compared with that independently obtained by continuum observations by JSD02.

The outline of the article is the following. In Sect. 2 we present the data, in Sect. 3 we describe the modeling of the observed lines and in Sect. 4 we discuss the physical and chemical structure of the envelope, namely the density and temperature profiles, as well as the abundances of the major species across the envelope. Besides, the central mass of the protostar and its accretion rate can also be constrained by these observations and modeling, yielding an alternative method to measure these two key parameters. In Sect. 4 we compare the results of the present study with previous studies of IRAS 4. Finally, we discuss the similarities and differences between IRAS 4 and IRAS 16293-2422, and highlight the importance of complementary ground-based, higher spatial and spectral resolution observations to understand the physical and chemical processes taking place in the innermost regions of low-mass envelopes.

2. Observations and results

A full-range spectral survey (43–196 μm) of the IRAS 4 region was performed using *LWS*. The observations were obtained on three positions in *LWS* grating mode, with a spectral resolution of about 200 (AOT LO1). The first position was centered in between IRAS 4A and IRAS 4B (α_{2000} = $03^h29^m11.9^s$, δ_{2000} = $31°13'20.3''$), and hence *LWS* 80″ beam includes both sources. The two other positions aimed to the lobe peaks of the outflow powered by IRAS 4: NE-red, α_{2000} = $03^h29^m15.6^s$, δ_{2000} = $31°14'40.1''$), and SW-blue, α_{2000} = $03^h29^m06.6^s$, δ_{2000} = $31°12'08.7''$). These observations, performed during revolution 847, are made of 30 scans on the central position and 10 scans on the two other positions. The sampling rate was 1/4 of the grating resolution element (0.29 μm in the 43–92 μm range, and 0.15 μm in the 84–196 μm range). The integration time for each sampled point was 12 s on the central position, and 4 s on the outflow positions.

The same data set has been previously analyzed by Ceccarelli et al. (1999) and Giannini et al. (2001, hereafter GNL01). We here report again the analysis of this dataset as we used an improved data processing module, allowing the correction of the transient effects that affect the LWS detectors (Caux 2001). As for standard pipeline products, the data are calibrated against Uranus, and the calibration uncertainty is estimated to be better than 30% (Swinyard et al. 1998). On the three observed positions, the spectra were then defringed for all ten detectors, and the continuum was removed fitting a polynomial baseline outside the lines. The data were then averaged over the ten detectors and binned at a single resolution to produce a single spectrum for each observed position. The line flux measurements were finally performed with the ISAP package, using gaussian fits. A particular attention was given to the determination of uncertainties associated with the line fluxes measurement. These are due to the statistical uncertainties, the absolute calibration and the baseline determination uncertainties that affect low resolution LWS observations. In grating mode, on a spectrum rich in lines as it is the case here, the line confusion may be important, making the baseline determination difficult. This uncertainty, often neglected in the literature, should be taken into account, as it can lead to important errors, especially for faint lines.

Figure 1 shows the observed 60–200 μm spectra in the three observed positions, and Table 1 reports the measured line fluxes. The errors quoted in this table include statistical errors, errors due to the uncertainty of the baseline removal, and an absolute calibration error of 30%. The first striking result of these observations is the dramatic difference within the three spectra: while that including IRAS 4A and 4B is very rich in CO and water lines, molecular emission is barely detected towards the outflow peaks (where the millimeter CO emission is the brightest). On the contrary, the fine structure [OI] 63 μm and [CII] 157 μm lines have comparable fluxes in the three observed positions. Finally, we wish to comment our results with respect to previous published data reductions. The present line flux determination agrees with that quoted by Ceccarelli et al. (1999) when considering the uncertainties. However, we note several differences with respect to the values quoted in GNL01. While there is a relatively good agreement between their fluxes of the strongest lines and ours (see Table 1), there is a noticeable discrepancy between our respective reductions regarding the weakest lines. We think that this is probably due to a too optimistic evaluation of the noise in GNL01. For example, in

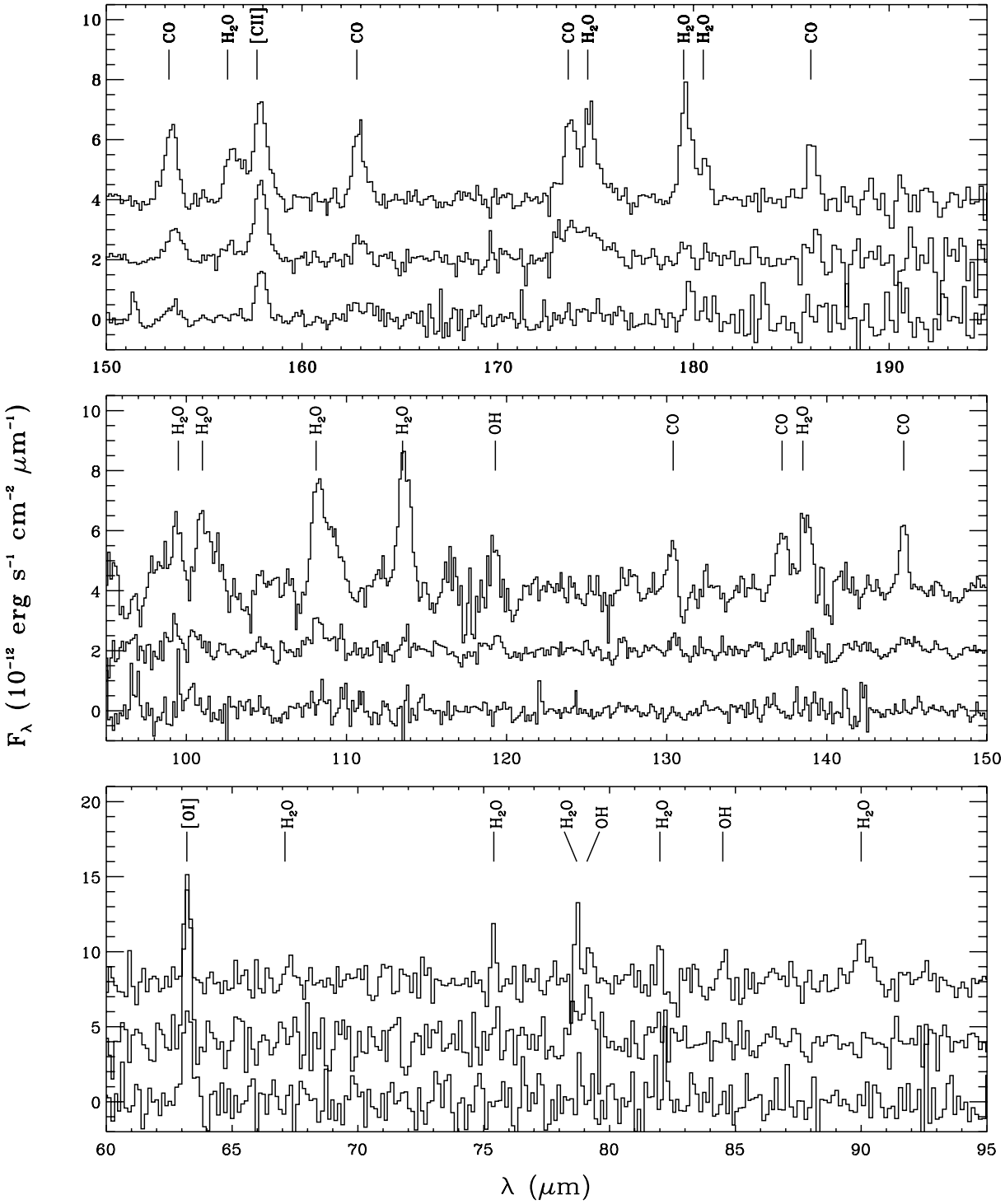

Fig. 1. ISO-LWS spectra observed towards IRAS 4 on source (top line), NE-red (middle line) and SW-blue (bottom line).

the NE-red position we find a statistical error around 175 μm of 1.5×10^{-13} erg s^{-1} cm^{-2} μm^{-1}, while Giannini et al. quote 2×10^{-14} erg s^{-1} cm^{-2} μm^{-1} in their Table 3. We do not confirm neither the detection of CO lines with $J_{\rm up} \geq 21$[2], nor the 125.4, 83.3, 66.4 and 58.7 μm water lines on-source. As shown in our Fig. 1, we only detected the 179.5 μm 174.6 μm and 108.0 μm lines in the outflow peak position NE-red, and the CO lines between $J_{\rm up}$ = 14 and 17. We also do not confirm their detections of CO $J_{\rm up} \geq 18$ lines in the NE-red outflow peak position. Finally, in the SW-blue position we only detected C^+ and OI 63 μm emission and very marginally the H_2O 179 μm lines.

[2] CO 21–20 is definitively undetected, CO 22–21 is blended with OH at 119 μm, while CO 23–22 and CO 24–23 are blended with water lines at 113.5 and 108.8 μm line respectively. One can note that the 108 μm is wider than expected, which could be due to the presence of the CO 24–23 line. Nonetheless, this detection would be inconsistent with the non detection of lower and higher J CO lines. Higher spectral resolution observations are needed to settle the question.

Table 1. Measured line fluxes in units of 10^{-12} ergs s^{-1} cm^{-2}. Upper limits are given as 2 σ.

Specie	Transition	Wavelength	E_{up}		Fluxes	
		(μm)	(cm^{-1})	On source	NE-red	SW-blue
o-H_2O	2_{21}-2_{21}	180.49	134.9	1.1 ± 0.5	<0.5	<0.5
	2_{12}–1_{01}	179.53	79.5	2.7 ± 1.0	0.5 ± 0.4	0.6 ± 0.4
	3_{03}–2_{12}	174.63	136.7	1.6 ± 0.7	0.5 ± 0.4	< 0.5
	4_{14}–3_{03}	113.54	224.5	3.0 ± 1.0	<0.5	<0.5
	2_{21}–1_{10}	108.07	134.9	2.0 ± 0.8	0.9 ± 0.5	<0.5
	5_{05}–4_{14}	99.48	325.3	1.4 ± 0.6	<0.5	<0.5
	6_{16}–5_{05}	82.03	447.3	1.2 ± 0.6	<0.5	<0.5
	4_{23}–3_{12}	78.74	300.5	1.4 ± 0.6	<0.5	<0.5
	3_{21}–2_{12}	75.38	212.1	1.7 ± 0.7	<0.5	<0.5
p-H_2O	3_{22}-3_{13}	156.19	206.3	0.5 ± 0.4	<0.5	<0.5
	3_{13}–2_{02}	138.53	142.3	1.2 ± 0.6	<0.5	<0.5
	2_{20}–1_{11}	100.98	136.2	1.0 ± 0.5	<0.5	<0.5
	3_{22}–2_{11}	89.99	206.3	1.4 ± 0.6	<0.5	<0.5
	3_{31}–2_{20}	67.09	285.1	0.6 ± 0.4	<0.5	<0.5
CO	14–13	186.00	403.5	1.3 ± 0.6	1.2 ± 0.4	<0.5
	15–14	173.63	461.1	1.5 ± 0.7	0.8 ± 0.4	<0.5
	16–15	162.81	522.5	1.7 ± 0.7	0.7 ± 0.4	<0.5
	17–16	153.26	587.7	1.7 ± 0.7	0.6 ± 0.5	<0.5
	18–17	144.78	656.8	1.3 ± 0.6	<0.5	<0.5
	19–18	137.20	729.7	1.3 ± 0.6	<0.5	<0.5
	20–19	130.37	806.4	1.2 ± 0.6	<0.5	<0.5
OH	$^2\Pi_{3/2,5/2}$–$^2\Pi_{3/2,3/2}$	119.33	83.7	1.0 ± 0.5	<0.5	<0.5
	$^2\Pi_{3/2,7/2}$–$^2\Pi_{3/2,5/2}$	84.51	201.9	1.1 ± 0.5	<0.5	<0.5
	$^2\Pi_{1/2,1/2}$–$^2\Pi_{3/2,3/2}$	79.15	126.3	1.1 ± 0.5	<0.5	<0.5
[OI]	$^3P_1$–$^3P_0$	145.48	227.7	<0.5	<0.5	<0.5
	$^3P_2$–$^3P_2$	63.17	158.7	2.2 ± 0.9	4.3 ± 1.5	2.2 ± 0.9
[CII]	$^2P_{3/2}$–$^2P_{1/2}$	157.74	63.7	2.2 ± 0.9	1.8 ± 0.7	1.1 ± 0.5

3. Line modeling

3.1. Origin of the FIR line emission

The molecular emission (H_2O, CO and OH) observed toward IRAS 4 can have at least three different origins: the two outflows powered by IRAS 4A and IRAS 4B, the PDR at the surface of the cloud, and the collapsing envelopes around the two protostars. The origin of the molecular line emission can be disentangled when the spatial distribution of the line emission and/or the line profiles are available. For example, lines arising in the envelope or in the molecular cloud have narrow profiles whereas lines arising from outflows show broadened profiles with extended wings. Unfortunately, in the case of the ISO-LWS observations, the relatively low spatial and spectral resolution do not allow to observationally disentangle the different components. However, the comparison between the central and the NE-red and SW-blue positions allows a first guess of the origin of the observed emission. The [OI] and [CII] lines have comparable line fluxes in the three observed positions. For this reason it is likely that the observed [OI] and [CII] emission is associated with the ambient diffuse gas, either emitted in the PDR or in the molecular cloud itself. On the contrary, only the lowest lying ($J_{up} \leq 17$) CO lines are detected on the NE-red position, while no H_2O or CO emission is clearly detected on the SW-blue position. On the other hand, the observations of the CO 3–2 line show that the high velocity gas (the fastest outflow component) peaks at the NE-red and SW-blue positions (Blake et al. 1995). The lack of water emission in these two outflow peak positions is not in favor of the hypothesis that the on-source water emission originates in the outflow. Although we cannot exclude a different origin and/or contamination for example from the densest parts of the outflow located in the ISO beam, in the following we explore the hypothesis of the envelope thermal emission and interpret the observed water line emission according to the CHT96 model. The first goal of our modeling is to verify that the thermal emission from the surrounding envelope can reproduce the water line observations, a necessary condition even though not sufficient to test this hypothesis. A following section will then address the possible origin of the CO and OH observed emission.

3.2. Model description

The CHT96 model computes in a self-consistent way the radiative transfer, thermal balance, and chemistry of the main gas coolants (i.e. O, CO and H_2O) across the envelope, in the *inside-out* framework (Shu 1977). Here we give a brief description of the main aspects of the model.

The initial state of the envelope is assumed to be an isothermal sphere in hydrostatic equilibrium, which density is given by:

$$n_{H_2}(r) = \frac{a^2}{2\pi\mu m_H G} r^{-2} \quad (1)$$

where a is the sound speed, $m_{\rm H}$ is the hydrogen mass, μ is the mean molecular mass, r the distance from the center and G the gravitational constant.

At $t = 0$ the equilibrium is perturbed and the collapse starts from inside out, propagating with the sound speed. The density in the inner collapsing region is given by the free-fall solution:

$$n_{\rm H_2}(r) = \frac{1}{4\pi\mu m_{\rm H}} \frac{\dot{M}}{(2GM_*)^{1/2}} r^{-3/2} \quad (2)$$

where M_* is the star mass, $\dot{M}$ is the accretion rate, related to the sound speed by:

$$\dot{M} = 0.975 \frac{a^3}{G}. \quad (3)$$

The free-fall velocity is given by:

$$v(r) = \left(\frac{2GM_*}{r}\right)^{1/2}. \quad (4)$$

The gravitational energy is released as material falls at the core radius R_*, so that the luminosity of the protostar is:

$$L_* = \frac{GM_*\dot{M}}{R_*}. \quad (5)$$

In the following L_* is the bolometric luminosity of IRAS 4, and we leave M_* and $\dot{M}$ as free parameters.

The radiative transfer in the envelope is solved in the escape probability approximation in presence of warm dust, following the Takahashi et al. 1983 formalism. The CHT96 model assumes that the initial chemical composition is that of a molecular cloud, and then it solves the time dependent equations for the chemical composition of 44 species, as the collapse evolves. H_2O, CO and O are of particular importance since they are the main coolants of the gas, and hence we study the chemistry of these species in detail. The CO molecule is very stable, and its abundance results constant across the envelope. H_2O is mainly formed by dissociative recombination of the H_3O^+ in the cold outer envelope, while, at dust temperature above 100 K, icy grain mantles evaporate, injecting large amounts of water into the gas phase. When the gas temperature exceeds ~250 K, the H_2O formation is dominated by the endothermic reactions O + H_2 → OH + H followed by H_2 + OH → H_2O + H, which transform all the oxygen not locked in CO molecules into H_2O.

From the above equations and comments, the water line emission depends on the mass of the central object, the accretion rate and the abundance of H_2O in the outer envelope and in the warm region, where its abundance is dominated by the mantle evaporation. All these quantities directly enter into the H_2O line emission, and specifically into the determination of the H_2O column density. In fact, the accretion rate sets the density across the protostellar region (Eqs. (1) and (2)). The central mass of the protostar affects the velocity field, and hence indirectly the line opacity (Eq. (4)). This parameter also sets the density in the free-fall region (Eq. (2)) and therefore the gas column density in this region. The water emission also depends indirectly on the O and CO abundances, which enter in the thermal balance and hence in the gas temperature determination. Several recent studies (Baluteau et al. 1997; Caux et al. 1999b; Vastel et al. 2000; Lis et al. 2001) have shown that almost the totality of the oxygen in molecular clouds is in atomic form. Accordingly, we assume the oxygen abundance to be the standard interstellar value, i.e. 5×10^{-4} with respect to H_2. With regard to the CO abundance, following Blake et al. 1995 we adopt a CO abundance of 10^{-5} with respect to H_2, lower than the standard abundance as this molecule is believed to be depleted on IRAS 4. We will comment later on the influence of these parameters on our results. Finally, the water abundance in the cold and in the warm parts of the envelope are poorly known and are free parameters in our study.

To summarize, we applied the CHT96 model to IRAS 4, and to reproduce the observations we varied the four following parameters: the mass of the central object M_*, the accretion rate $\dot{M}$, the water abundance in the outer cold envelope $X_{\rm out}$, and the water abundance in the region of mantle evaporation $X_{\rm in}$. The principal limitation to the application of this model to IRAS 4 is that the ISO beam includes both IRAS 4A and IRAS 4B envelopes. As a first approximation, we assumed that the two envelopes contribute equally to the molecular emission. Finally we assumed that the two envelopes touch each other, namely they have a radius of 3000 AU (i.e. 30″ in diameter), in agreement with millimeter continuum observations (Motte & André 2001). In our computations we adopted a distance of 220 pc in agreement with JSD02 and a luminosity of 5.5 $L_\odot$ for each protostar, according to Sandell et al. (1991) when assuming such a distance.

3.3. Water line modeling results

In order to constrain the mass, accretion rate and water abundance across the envelope, we run several models varying the central mass from 0.3 to 0.8 $M_\odot$, the accretion rate from 10^{-5} to 10^{-4} $M_\odot\,{\rm yr}^{-1}$, the water abundance in the outer parts of the envelope $X_{\rm out}$ between 10^{-7} and 10^{-6}, and a water abundance in the inner parts of the envelope $X_{\rm in}$ between 10^{-6} and 2×10^{-5} respectively. In the following we discuss the results of this modeling.

3.3.1. Accretion rate and water abundance in the outer parts of the envelope

One of the difficulties in constraining the central mass, accretion rate and water abundance in the envelope is that the water line intensity a priori depends on all the parameters. However, choosing appropriate lines can help constraining one parameter at once. Low lying H_2O lines are expected to rapidly become optically thick in the outer envelope, where they are easily excited. Hence these lines depend weakly on $X_{\rm in}$ and M_* (which affect the line emission in the collapsing inner region). We therefore used the low-lying lines to constrain the other two parameters, namely $X_{\rm out}$ and $\dot{M}$. For this we minimized the $\chi^2 = \frac{1}{N-1}\sum_1^N \frac{({\rm Observations-Model})^2}{\sigma^2}$ obtained considering only water lines having a $E_{\rm up}$ lower than 142 cm^{-1}, and where σ is the error associated with each line flux. Figure 2 shows the χ^2 surface as a function of $X_{\rm out}$ and $\dot{M}$ for $M_* = 0.5\ M_\odot$. We obtained a similar plot for $M_* = 0.3\ M_\odot$ and the result is basically

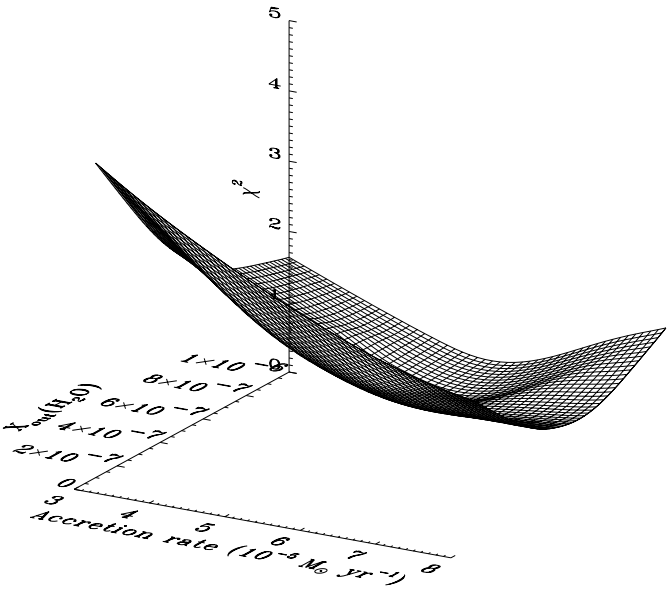

Fig. 2. χ^2 surface as function of the water abundance in the outer envelope $X_{\rm out}$ and the mass accretion rate $\dot{M}$. The χ^2 has been obtained considering the lines with an upper level energy $E_{\rm up}$ lower than 142 cm^{-1} and for a central mass of 0.5 $M_\odot$.

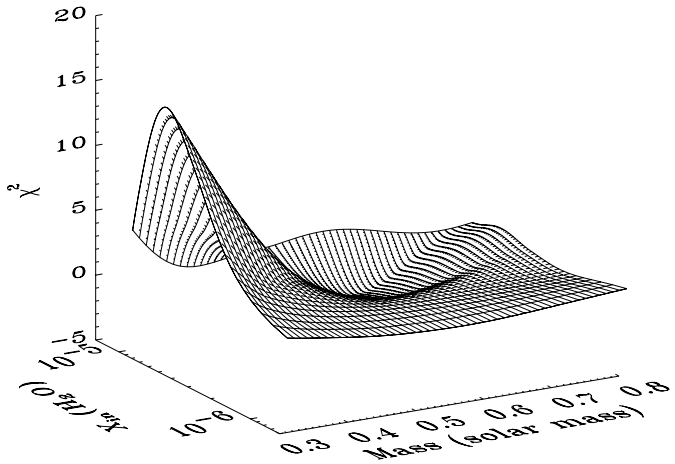

Fig. 3. χ^2 surface as function of the central mass $M_*$and water abundance in the innermost parts of the envelope $X_{\rm in}$. The χ^2 has been obtained considering the lines with an upper level energy $E_{\rm up}$ larger than 142 cm^{-1} and assuming $\dot{M} = 5\times10^{-5}$ and $X_{\rm out} = 5\times10^{-7}$. Note that we did not include the 82 and 99.5 μm lines, which seems underestimated by our model (see text). We did not include the 113 μm line either, because of the blending with the CO $J_{\rm up}$ = 23 line, which makes the estimate of the flux rather uncertain.

the same. As suspected, the chosen lines constrain relatively efficiently the two parameters $X_{\rm out}$ and $\dot{M}$. The minimum χ^2 is obtained for a water abundance $X_{\rm out} \sim 5\times10^{-7}$ and an accretion rate $\dot{M} \sim 5\times10^{-5}$ $M_\odot$ yr^{-1}.

3.3.2. Central mass and water abundance in the inner parts of the envelope

We then constrained the central mass M_* and the abundance in the innermost parts of the envelope $X_{\rm in}$ using the high-lying lines. In fact to be excited, these lines require relatively high temperatures and densities which are likely to be reached only in the innermost parts of the envelope. Their intensities depend hence on the water abundance $X_{\rm in}$ in these parts and on the central mass M_*. The χ^2 surface as function of these two parameters is shown in Fig. 3, obtained considering the lines having an upper level energy $E_{\rm up}$ larger than 142 cm^{-1}, and assuming $\dot{M} = 5\times10^{-5}$ and $X_{\rm out} = 5\times10^{-7}$. In this case the χ^2 has a minimum around $M_* = 0.5$ $M_\odot$ and $X_{\rm in} = 5\times10^{-6}$. Specifically, if we adopt a constant H_2O abundance of 5×10^{-7} ($X_{\rm out}$) across the entire envelope, the model predicts intensities a factor between two and five lower than those observed (high lying lines, i.e. with $E_{\rm up} \geq 250$ K). In other words, the observed emission can only be accounted for if a jump in the water abundance is introduced when the dust temperature exceeds 100 K, the sublimation temperature of icy mantles. This jump has to be larger than about a factor 10.

3.3.3. The best fit model

Assuming two identical envelopes, the best fit model is obtained with a central mass of 0.5 $M_\odot$, accreting at 5×10^{-5} $M_\odot$ yr^{-1} (Table 2).

Table 2. Best fit parameters and derived quantities for IRAS 4 and comparison with the values obtained towards IRAS 16293-2422 by Ceccarelli et al. (2000a).

Parameter	IRAS 4	IRAS 16293-2422
Mass ($M_\odot$)	0.5	0.8
Accretion rate ($M_\odot$ yr^{-1})	5×10^{-5}	3×10^{-5}
Water abundance $X_{\rm out}$	5×10^{-7}	3×10^{-7}
Water abundance $X_{\rm in}$	5×10^{-6}	3×10^{-6}
Radius ($T_{\rm dust}$ = 30 K) (AU)	1500	4000
Radius ($T_{\rm dust}$ = 100 K) (AU)	80	150
Age (yr)	1.0×10^4	2.7×10^4

Assuming a constant accretion rate, this gives an age of 10 000 years, close to the dynamical age of the outflows. The abundance of water in the outer parts of the envelope is 5×10^{-7} and it is enhanced by a factor 10 in the innermost regions of the envelope, where grain mantles evaporate. Figure 4 shows the ratio between the observed and predicted line fluxes as function of the upper level energy of the transition. The model reproduces reasonably well the observed water emission, with the exception of the lines at 99.5 μm and 82.0 μm that seems to be underestimated (by a factor 10) by our model.Since, on the contrary, lines in a comparable range of $E_{\rm up}$ are well reproduced by our model, we think that this discrepancy is likely due to a rough baseline removal. Specifically, the estimate of both the 99.5 and 82.0 μm line fluxes may suffer of an incorrect baseline removal, as the lines lie on the top of a strong dust feature, which covers the 80–100 μm range (Ceccarelli et al. in preparation). Higher spectral resolution observations are required to confirm this explanation. Finally some unexplained discrepancy between the model and the observations may exist at the higher values of $E_{\rm up}$.

In the figure we also report different symbols for the ortho and para water transitions respectively. In our model we

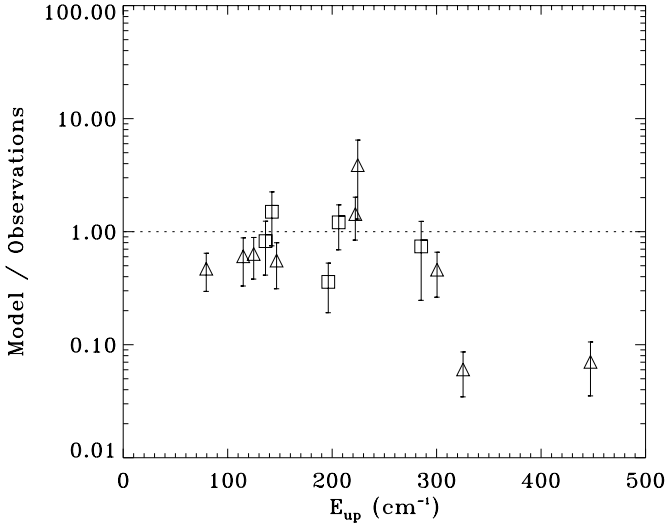

Fig. 4. Ratio between the line fluxes predicted by our best fit model and observed ones as function of the upper level energy of the transition $E_{\rm up}$. Triangles represent ortho H_2O transitions, and squares represent para H_2O transitions. Note that the model assumes an ortho to para ratio equal to 3.

assumed that this ratio is equal to 3. The comparison between the observations and predictions is consistent with this assumption. Plots of the predicted intensity of various lines as function of the radius are reported in Fig. 5. Finally, the envelope model predicts an intensity of 1.8×10^{-13} erg s^{-1} cm^{-2} and a linewidth of $\sim$1 km s^{-1} for the ground water line at 557 GHz, equivalent to an antenna temperature of 30 mK in the SWAS beam ($\sim$4′). SWAS detected a $T_{\rm a}^{*}$ $\sim$ 100 mK line, which linewidth is $\sim$18 km s^{-1}, and self-absorbed at the rest velocity (Bergin et al. 2002). The observed line is undoubtedly dominated by the outflow emission, and only a small fraction of its intensity can be attributed to the envelope emission, in agreement with our model predictions.

3.4. [OI], [CII], OH and CO emission

[OI] 63 μm and [CII] 157 μm emission is widespread, and probably associated with the cloud. A plausible explanation is that the two lines are emitted in the PDR resulting from the UV and/or X-ray illumination of this cloud from the several young stars that it harbors. The comparison of the observed fluxes with the model by Kaufman et al. (1999) suggests a PDR with a density of about 10^4 cm^{-3} and a incident FUV of $\sim$5 G_0. This PDR would account for the total observed flux of the [CII] 157 μm line and OI. The parameters we derive are in agreement with those quoted by Molinari et al. (2000), who studied the region around SVS13.

The thermal emission from the envelope predicts no C^+ emission, of course, as no source of ionization is considered in the CHT96 model. The atomic oxygen, on the contrary, is present all along the envelope and it is predicted to emit 1.8×10^{-12} erg s^{-1} cm^{-2}. This is similar to the observed [OI] 63 μm flux. The fact that we do not see any [OI] 63 μm enhancement towards the source with respect to the surroundings

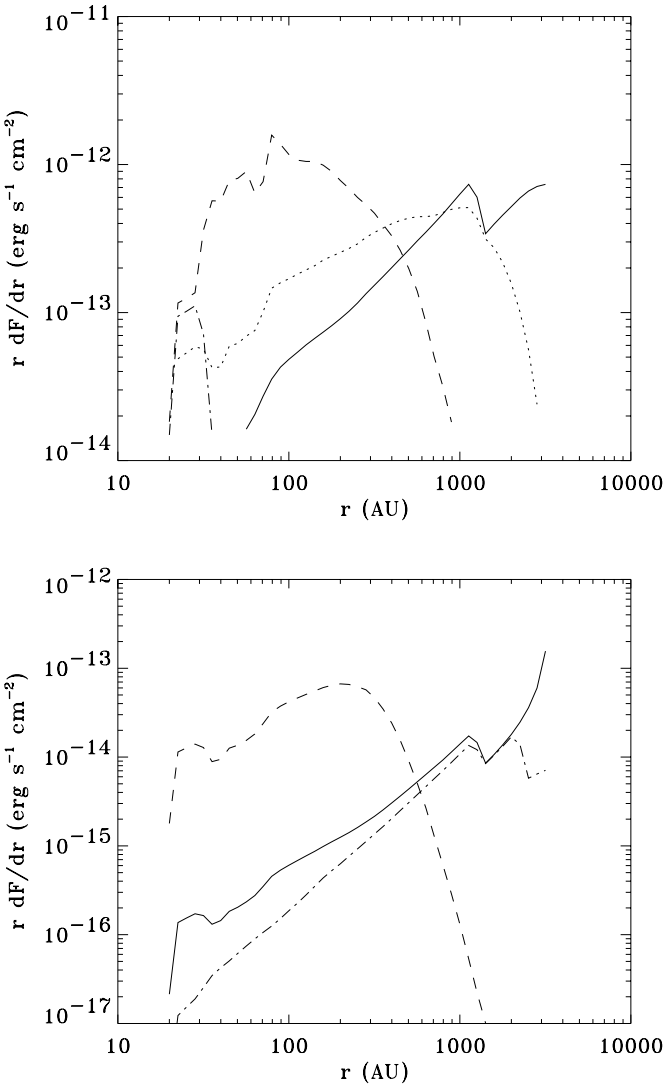

Fig. 5. Predicted intensity of various lines as function of the radius. The upper panel shows the water lines at 179 μm (solid line), 108 μm (dotted line), 75 μm (dashed line) and 82 μm (dash-dotted line). The lower panel shows the CO $J_{\rm up}$ = 3 (solid line), CO $J_{\rm up}$ = 14 (dashed line) and $C^{18}O$ $J_{\rm up}$ = 3 (dash-dotted line).

can be explained if IRAS 4 is well embedded in the parental cloud. Being the ground transition, the [OI] 63 μm line is relatively easily optically thick, and an emission from an embedded source can be totally absorbed by the foreground material (Poglitsch et al. 1996; Baluteau et al. 1997; Caux et al. 1999b; Vastel et al. 2000).

Finally, our model predicts OH and CO $J_{\rm up} \geq 14$ line fluxes more than ten times lower than those observed. Note that the FIR CO lines predicted by the CHT96 model are optically thick and not sensitive to the adopted abundance, and therefore increasing the CO abundance would not change the result. An extra heating mechanism is evidently responsible for the excitation of the FIR CO lines observed in the central position. Shocks have been invoked in the literature (e.g. Ceccarelli et al. 1998; Nisini et al. 1999; Giannini et al. 2001), but this hypothesis has its own drawbacks and flaws (see Introduction). Another possibility is that the FIR CO lines are emitted in a

superheated layer of gas at the surface of a flaring disk, as seen in the protostar El 29 (Ceccarelli et al. 2002), and/or at the inner interface of the envelope itself (Ceccarelli, Hollenbach, Tielens et al. in preparation). In the first case (disk surface), the gas is "super-heated" because the grain absorptivity in the visible exceeds the grain emissivity in the infrared (e.g. Chiang & Goldreich 1997). In the latter case (envelope inner interface) the extra heating is provided by the X-ray photons from the central source. A full discussion about the FIR CO emission origin is beyond the scope of this article and we refer the interested reader to the above mentioned articles.

4. Discussion

4.1. The structure of the envelope

The first result of our modeling is its capacity to reproduce the observed water emission. In the following we show that the derived parameter values are in agreement with previous estimates obtained through different studies. Before discussing in detail this comparison we describe here the derived density and temperature profiles, as well as the gas heating and cooling mechanisms. The reconstructed density and temperature profiles are shown in Fig. 6. In the outer region the density follows a r^{-2} law (static region), while in the inner region the density is proportional to $r^{-3/2}$ (free-fall region), with a transition region starting at ∼1500 AU, that covers a substantial range of radii and is flatter than $r^{-3/2}$. The absolute density is relatively large, 4×10^6 cm^{-3} at 1500 AU.

The gas temperature closely follows the dust temperature in the outer and intermediate regions of the envelope. At $r \sim$ 80 AU, dust and gas decouple. This is caused by the evaporation of the icy mantles when the dust temperature reaches 100 K, which injects large amounts of water in the gas phase (about a factor ten more) increasing the cooling efficiency of the gas. The gas temperature drops by about 20 K and remains lower than the dust temperature until at $r \sim 30$ AU the dust FIR pumping of the water molecules counterbalances the water line cooling and couples again the gas and dust temperatures. The heating and cooling of the gas in the envelope follow the general properties discussed in CHT96 (see also Ceccarelli et al. 2000a). The heating is dominated by the NIR water pumping, gas-grains collisions and the compression of the gas in the innermost regions, while gas-dust collisions are the main heating factor in the outer parts of the envelope and when the dust and gas decouple at $r \sim 80$ AU. The gas cooling is dominated by the line emission of water, oxygen and CO. In the outer parts of the envelope the cooling is dominated by the CO line emission, while in the intermediate region the cooling is dominated by the oxygen and water lines, as the CO lines become rapidly thick. At $r \leq 80$ AU, the cooling by the water lines takes over, due to the icy mantle evaporation, and dominates the cooling by orders of magnitude with respect to O and CO. Note that before the ices evaporation (i.e. at $r \geq 80$ AU), the heating is dominated by the gas compression and the cooling by the H_2O line emission. The increase of the gaseous water abundance by a factor ten causes an increase of about the same amount in the gas cooling rate, whereas the compression heating rate just

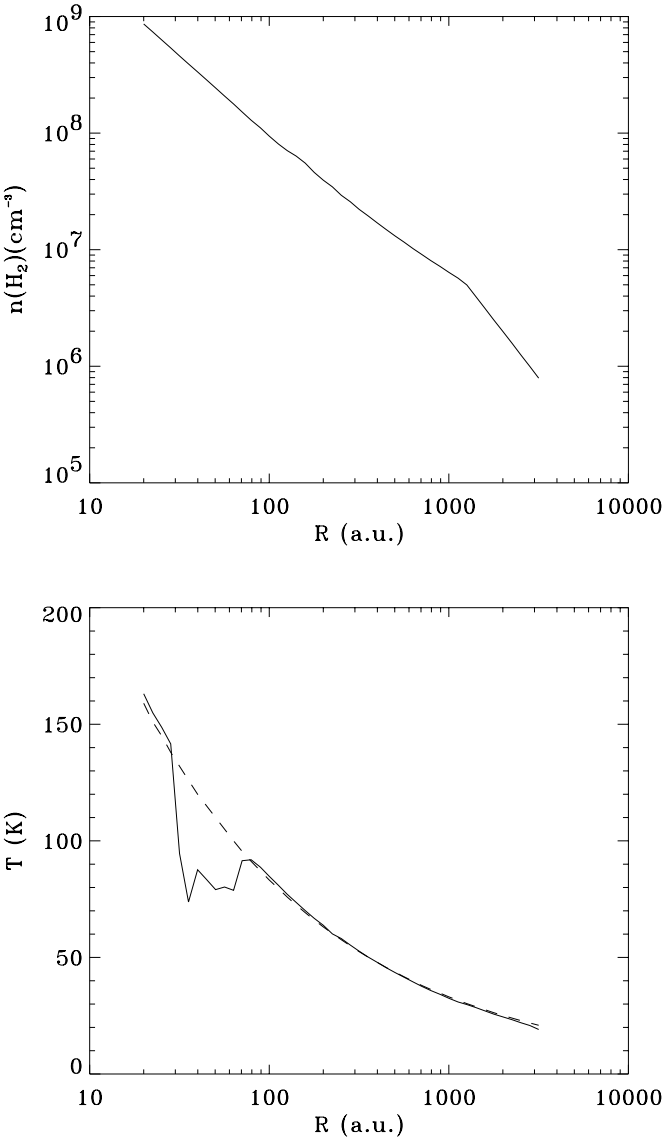

Fig. 6. Density and temperature profiles of the envelope as computed by the best fit model. In the lower panel the dashed line refers to the dust temperature, while the solid line refers to the gas temperature.

increases by 20%. The gas heating becomes hence dominated by the gas-grains collisions, which tend to couple dust and gas. In the specific case of IRAS 4, the water cooling rate Λ_{H_2O} and gas-grains collisions heating rates Γ_{dg} can be approximated by the following expressions, at the radius just before the evaporation (for the details see CHT96):

$$\Lambda_{H_2O} = 3.4 \times 10^{-15} \frac{x(H_2O)}{5 \times 10^{-7}} \left(\frac{T_{gas}}{90\ K}\right)^{3/2} \text{erg s}^{-1}\text{cm}^{-3} \quad (6)$$

$$\Gamma_{dg} = 3.6 \times 10^{-16} (T_{dust} - T_{gas}) \left(\frac{T_{gas}}{90\ K}\right)^{1/2} \text{erg s}^{-1}\text{cm}^{-3}. \quad (7)$$

The increase of a factor ten in the water cooling rate after the ice evaporation is only in partly counter-balanced by the increased heating rate due to the gas-grains collisions, and the difference between the two temperatures is ∼20 K.

The CO and atomic oxygen abundances are constant across the envelope, within the studied range, i.e. 30 to 3000 AU.

We will discuss in the next paragraph the effect of varying the CO abundance across the envelope to take into account the CO depletion when the dust temperature is below the CO-rich ice evaporation temperature. As widely discussed previously, the water abundance undergoes a jump of about a factor ten at $r \leq 80$ AU, when H_2O-rich ices evaporate (dust temperature larger than 100 K).

One interesting prediction of this study is the existence of a hot core like region in the innermost parts of the envelope, where the dust temperature reaches the sublimation temperature of the grain mantles.

4.2. CO depletion

Here we want to address in some detail the issue of the CO depletion claimed in IRAS 4 by comparing low-lying, millimeter CO transitions and dust continuum emission (Blake et al. 1995). Blake et al. used the CO $J = 3{-}2$ transitions of the ^{12}C, ^{18}O and ^{17}O isotopes and found that the emission is accounted for a CO abundance of $\sim 2.5 \times 10^{-5}$, i.e. a factor five lower than the "canonical" value. Their explanation is that CO molecules freeze out on the grain mantles and the gas phase CO results therefore depleted across the envelope. This result has been recently confirmed by JSD02, who quote $CO/H_2 \sim 10^{-5}$ in the outer envelope of IRAS 4. The question arises whether the CO is depleted across the entire envelope or not, as also remarked by JSD02. We checked with our model if the millimeter observations would be sensitive to higher abundances of CO in regions where the dust temperature exceeds the CO-rich ice evaporation temperature, i.e. ~25–30 K. We found that if the $C^{18}O$ $J = 3 - 2$ line is optically thin, the bulk of the $J = 3 - 2$ line is emitted at ~3000 AU. This is because of the excitation of the CO $J = 3 - 2$ line itself. In the optically thin and thermalized line approximation it is possible to derive the following approximate analytical expression (strictly speaking, valid only for the CO millimeter lines):

$$I_J \propto \int \frac{\exp[-E_J/kT_{\rm gas}]}{T_{\rm gas}} {\rm d}r. \quad (8)$$

When $J = 3$ the integrand has a peak around $T_{\rm gas} \sim 30$ K, does not vary by more than 20% with temperatures between 20 K and 40 K, and decreases for temperatures larger than ~40 K. As a result, the line intensity in the outer envelope is linearly proportional to the radius of the emitting gas, and therefore increases going outward, i.e. the emission is dominated by the outer envelope where CO is depleted.

We run a case in which there is no CO depletion across the envelope, (i.e. the CO abundance is constant and equal to 10^{-4}), a case where CO is depleted on the entire envelope (i.e. the CO abundance is constant and equal to 2.5×10^{-5}), and a third case where CO is depleted only in the outer envelope (i.e. the CO abundance is 1×10^{-5} when $T_{\rm dust} \leq 30$ K and 10^{-4} in the rest of the envelope). The last two cases give the same intensity (within 15%) on both $C^{18}O$ $J = 3 - 2$ and $J = 2 - 1$ lines, while the first one gives an intensity larger by about a factor 3. Therefore, the last two cases, CO depletion across the entire envelope and depletion in the outer envelope only, are not distinguishable by the $C^{18}O$ $J = 3 - 2$ and $J = 2 - 1$ observations. In this sense, we think that the $J_{\rm up} \leq 3$ observations cannot probe the innermost regions and that it is possible that the measured CO depletion is only relative to the external regions of the envelope.

This situation would be similar to what has been claimed to occur in IRAS 16293-2422 (Ceccarelli et al. 2001), based on the indirect evidence provided by the D_2CO emission. The D_2CO molecule is considered a grain mantle product, as gas phase reactions seem unable to form an appreciable amount of this molecule. Ceccarelli et al. showed that in IRAS 16293-2422 the D_2CO emission originates in the region of the envelope where $T_{\rm dust} \geq 30$ K. The proposed interpretation is that D_2CO is trapped in CO-rich ices that evaporate when the dust temperature exceeds 30 K. Hence, in IRAS 16293-2422 there is an outer region of the envelope where CO is frozen onto the grain mantles ($T_{\rm dust} \leq 30$ K), and a regions with $T_{\rm dust} \geq 30$ K where CO is released into the gas phase and has the standard $\sim 10^{-4}$ abundance. A similar scenario has been also suggested by JSD02 for other Class 0 sources that show CO depletion.

4.3. Comparison with previous studies of IRAS 4

In this paragraph we compare our results with previous studies dealing in a way or in another with some of the issues addressed in the present study. We start with the recent study by JSD02, who derived the density profile of the IRAS 4 envelopes by modeling the continuum emission (spectral energy distribution and 450/850 μm maps simultaneously) and assuming a single power law index. They found a power law index equal to 1.8 and 1.3 for 4A and 4B respectively, consistent with the Shu inside-out solution adopted in our model. At 1000 AU they estimate a density equal to 6 (4A) and 2 (4B) $\times 10^6$ cm^{-3}, which are quite comparable with our estimate: 6×10^6 cm^{-3}. We emphasize that the two methods, their and our, are totally independent, and use different data, continuum and line observations respectively. The fact that both predict approximately the same density structure in a certain way validate both methods, or at least increases the probability that both models describe reasonably well IRAS 4.

Apart from the density and temperature profiles, our model also constrains the water abundance profile. It is reasonable to ask whether our predicted water abundance in the innermost and outer regions of the envelope are realistic and if they have any support from different observations. The situation here is somewhat complicated by the fact that there aren't many other independent ways to measure the water abundance. From a theoretical point of view the abundance in the outer envelope, 5×10^{-7}, can be very well compared with chemistry model predictions (e.g. Lee et al. 1996). In this respect, the value that we derive is certainly not extraordinary and rather plausible. From an observational point of view Bergin et al. (2002) succeeded to detect the 557 GHz water line in the NGC1333 molecular cloud. They estimate the water abundance in the region to be $\sim 10^{-7}$, with unfortunately a relatively large error (~10) due to the many uncertainties in the excitation of the line. Moneti et al. (2001) derived a water abundance of 3×10^{-7} in the clouds in the line of sight of the galactic center. These authors claim that

this is very likely the abundance of standard molecular clouds. In summary, the water abundance that we find for the cold region of the IRAS 4 envelope is consistent with other studies. Regarding the abundance in the inner region, 5×10^{-6}, the value that we obtain seem to be lower than what expected if all the water ice is injected in the gas phase and a large fraction of the oxygen is locked in this ice. A typical water ice abundance is estimated around 10^{-4} (Tielens et al. 1991). However, SWAS observations of IRAS 4 and other low mass protostars suggest that the water abundance in their outflows is around 10^{-6} (Neufeld et al. 2001; Bergin et al. 2002), i.e. similar to the value that we find. Those estimates are very rough and could easily be off by a factor ten (Neufeld et al. 2000), as they are based on one transition only, but nevertheless have the advantage that the observed emission is certainly dominated by the outflow (the spectral resolution of these observations is $\sim$1.2 km s^{-1}) so there are no doubts on its origin. Since the water abundance in the outflow would be probably dominated by the grain mantles released in the gas phase, these observations probably measure the water content in the mantles, very much as our observations measure (indirectly) the water content mantles in the inner hot like region. The two measurements seem to be consistent in giving a rather low value. Whether this validates both measures is less certain than the density profile case: it certainly does not discredit the two measures. Finally, even the comparison of our estimate of the accretion rate and central mass are in good agreement with the previous estimates, based on a different method (line profile and molecule H_2CO), by Di Francesco et al. (2001). We derived $\dot{M} = 5 \times 10^{-5}\ M_\odot\,\mathrm{yr}^{-1}$ against the $11{-}4 \times 10^{-5}\ M_\odot\,\mathrm{yr}^{-1}$ quoted by Di Francesco et al. (2001), and $M_* = 0.5\ M_\odot$ against the 0.23–0.71 $M_\odot$.

To conclude, these studies show that the values we derive of the four parameters of our model are plausible and nothing of particularly surprising, with the possible exception of the water abundance in the innermost regions. In other words, if we had to choose a priori those values we would have chosen exactly what we found. The conclusion is that it is very probable that at least most of the observed water emission in IRAS 4 originates in the envelopes. If any, just a small fraction should therefore be associated with the outflow. Our final comment is therefore that care should be taken when interpreting the observed water emission towards low mass, Class 0 protostars as due to shocks (e.g. Ceccarelli et al. 1998; Nisini et al. 1999, GNL01), as we showed in two out two cases that the massive envelopes surrounding these sources dominate the water emission, just because of the large total column density. As a matter of fact, Class I sources, which are characterized by less massive envelopes, do not show up strong water emission (Ceccarelli et al. 2000a).

4.4. Comparison with IRAS 16293-2422

The mass and accretion rate we derived for IRAS 4A and B are of the same order of magnitude of those found in IRAS 16293-2422 (Ceccarelli et al. 2000a). IRAS 16293-2422 seems more massive (0.8 $M_\odot$) than IRAS 4A (0.5 $M_\odot$), and accreting at a slightly lower accretion rate (3 against 5 $\times10^{-5}\ M_\odot\,\mathrm{yr}^{-1}$). Assuming a constant accretion rate, those values give an age of 10 000 years and 27 000 for IRAS 4 and IRAS 16293-2422 respectively. Hence IRAS 16293-2422 seems more evolved than IRAS 4. Moreover, IRAS 4 possesses an hot core like region about two times smaller than IRAS 16293-2422 (80 AU against 150 AU). Ground-based H_2CO and CH_3OH observations (Blake et al. 1995; Maret et al. in preparation) confirm that IRAS 4 is in fact colder, and therefore less bright in these molecular transitions than IRAS 16293-2422, and that indeed the IRAS 4 hot core like region is very small. This fact coupled with the larger distance of IRAS 4 from the Sun may explain the apparent difference in the molecular emission of these two sources, which is much richer in IRAS 16293-2422. This conclusion is also in agreement with the relatively higher millimeter continuum observed in IRAS 4, which implies a larger amount of cold dust surrounding this source than IRAS 16293-2422. In addition, the region where the dust temperature is higher than 30 K is smaller in IRAS 4 ($\sim$1500 AU) than in IRAS 16293-2422 ($\sim$4000 AU), i.e. the CO depleted part of the envelope is relatively larger in IRAS 4 than in IRAS 16293-2422. This may explain why the CO depletion has been observed towards IRAS 4 and not in IRAS 16293-2422 (van Dishoeck et al. 1995; Ceccarelli et al. 2000b).

Finally, despite this difference in the age, the water abundance in the envelope is remarkably similar in the two sources, both in the outer part of the envelope and in the inner ones, where ice mantles are predicted to evaporate. This is an important piece of information, suggesting that the ice mantle formation in the two sources underwent a similar process, despite the macroscopic difference between the two molecular clouds which the two sources belong to. In the case of IRAS 16293-2422, the cloud seems very quiescent, shielded from strong UV and/or X-ray radiation (e.g. Castets et al. 2001) and with even evidence of large CO depletion (Caux et al. 1999b). In the other case, IRAS 4, the cloud presents cavities excavated by the several young stars of the region (e.g. Lefloch et al. 1998), and it is probably permeated by the X-rays emitted by them. A forthcoming study will allow to measure the H_2CO and CH_3OH abundances in the inner hot core like region of IRAS 4 (Maret et al. in preparation) and make comparisons with that found in IRAS 16283-2422 (Ceccarelli et al. 2000b). This study will hence help to understand in more detail how apparently different conditions in the parental clouds affect the grain mantle composition.

5. Conclusions

We presented a spectral survey of the protobinary system IRAS 4 in the NGC 1333 cloud, using ISO-LWS in grating mode. We targeted the source as well as two adjacent positions, NE-red and SW-blue, that encompass the red and blue lobes of the outflow emanating from IRAS 4, respectively. The three spectra are dominated by the [OI] 63μm and CII [157] μm lines, that likely originate in the PDR associated with the parental cloud. On the contrary, water emission is only detected towards

the on-source position, whereas no significant water emission is detected towards the NE-red and SW-blue positions. This suggests that the bulk of the water emission is due to the thermal emission of the protostellar envelopes around the two protostars. Using an accurate model of the chemistry, thermal balance and radiative transfer in protostellar envelopes (CHT96), we modeled the water line emission due to two identical envelopes surrounding IRAS 4A and B respectively. We found that the observations are consistent with the CHT96 model, which implicitly assumes the "inside-out" theory (Shu 1977). The best fit of the model allows us to estimate the four main model parameters: the accretion rate, $5\times10^{-5}\ M_{\odot}\ \mathrm{yr}^{-1}$, the central mass, 0.5 $M_{\odot}$, the water abundance in the outer envelope, 5×10^{-7}, and in the inner envelope, 5×10^{-6} (this last parameter is the least constrained with about a factor 3 of uncertainty). This gives an age of 10 000 years, assuming that the accretion rate remains constant during the collapse. Based on this model, we derived the density and temperature profiles of the gas in the envelopes. We also reviewed the suggestion by Blake et al. (1995) that CO is depleted by about a factor ten in the envelope of IRAS 4. We could not confirm or rule out this hypothesis but caution that the transitions used by this study, $C^{18}O$ 3–2 and 2–1, can hardly probe the inner regions, where the CO abundance may be "canonical".

A comparison with several previous studies of the same source (Blake et al. 1995; Neufeld et al. 2000; DiFrancesco et al. 2001, JSD02) shows that the derived parameters are reasonable and consistent with the available literature, hence re-enforcing the thesis that the observed water emission is indeed due to the thermal emission from the envelopes. A by-product of the present study is the prediction of the existence of a hot core like region in the inner parts of the envelope, where grain mantles evaporate, releasing large amounts of water (about a factor ten) in the gas phase. Such a hot core has already been proposed to exist around IRAS 16293-2422, where a similar study as been carried out (Ceccarelli et al. 2000a; Ceccarelli et al. 2000b). Comparison between the two protostars, show that IRAS 4 is younger and surrounded by a more massive envelope. This explains the larger continuum emission and the larger depletion factors observed in IRAS 4. Finally, this study emphasis the necessity of ground based observations, where higher spatial and spectral resolutions are achievable. H_2CO and CH_3OH are of particular interest as they are among the most abundant components of grain mantles, and are therefore expected to evaporate in the inner parts of the envelope. Appropriate transitions can hence be used to constrain the physical and chemical conditions in the innermost part of protostellar envelopes (see Ceccarelli et al. 2000b).

Acknowledgements. We wish to thank Edwin A. Bergin for frank and constructive discussions on the SWAS data. We thank Edwin A. Bergin and Jes K. Jørgensen for providing us with their papers prior to publication. The referee Neal Evans is thanked for his useful comments. Most of the computations presented in this paper were performed at the Service Commun de Calcul Intensif de l'Observatoire de Grenoble (SCCI).

References

Andre, P., Ward-Thompson, D., & Barsony, M. 1993, ApJ, 406, 122
Bachiller, R., & Perez Gutierrez, M. 1997, ApJ, 487, L93
Baluteau, J.-P., Cox, P., Cernicharo, J., et al. 1997, A&A, 322, L33
Bergin, E. A., Kaufman, M. J., Melnick, G. J., Snell, L. S., & Howe, J. E. 2002, ApJ, accepted
Blake, G. A., Sandell, G., van Dishoeck, E. F., et al. 1995, ApJ, 441, 689
Caselli, P., Hartquist, T. W., & Havnes, O. 1997, A&A, 322, 296
Castets, A., Ceccarelli, C., Loinard, L., Caux, E., & Lefloch, B. 2001, A&A, 375, 40
Caux, E. 2001, in The Calibration Legacy of the ISO Mission, E47
Caux, E., Ceccarelli, C., Castets, A., et al. 1999a, in ESA SP-427: The Universe as Seen by ISO, vol. 427, 643
Caux, E., Ceccarelli, C., Castets, A., et al. 1999b, A&A, 347, L1
Ceccarelli, C., Boogert, A. C. A., Tielens, A. G. G. M., et al. 2002, A&A, accepted
Ceccarelli, C., Castets, A., et al. 2000a, A&A, 355, 1129
Ceccarelli, C., Caux, E., Loinard, L., et la. 1999, A&A, 342, L21
Ceccarelli, C., Caux, E., White, G. J., et al. 1998, A&A, 331, 372
Ceccarelli, C., Hollenbach, D. J., & Tielens, A. G. G. M. 1996, ApJ, 471, 400
Ceccarelli, C., Loinard, L., Castets, A., et al. 2000b, A&A, 357, L9
Ceccarelli, C., Loinard, L., Castets, A., et al. 2001, A&A, 372, 998
Cernis, K. 1990, Ap&SS, 166, 315
Charnley, S. B., Tielens, A. G. G. M., & Millar, T. J. 1992, ApJ, 399, L71
Chiang, E. I., & Goldreich, P. 1997, ApJ, 490, 368
Choi, M., Panis, J., & Evans, N. J. 1999, ApJS, 122, 519
Clegg, P. E., Ade, P. A. R., Armand, C., et al. 1996, A&A, 315, L38
de Zeeuw, P. T., Hoogerwerf, R., de Bruijne, J. H. J., Brown, A. G. A., & Blaauw, A. 1999, AJ, 117, 354
Di Francesco, J., Myers, P. C., Wilner, D. J., Ohashi, N., & Mardones, D. 2001, ApJ, 562, 770
Doty, S. D., & Neufeld, D. A. 1997, ApJ, 489, 122
Evans, N. J. 1999, ARA&A, 37, 311
Giannini, T., Nisini, B., & Lorenzetti, D. 2001, ApJ, 555, 40
Gregersen, E. M., Evans, N. J., Zhou, S., & Choi, M. 1997, ApJ, 484, 256
Herbig, G. H., & Jones, B. F. 1983, AJ, 88, 1040
Jennings, R. E., Cameron, D. H. M., Cudlip, W., & Hirst, C. J. 1987, MNRAS, 226, 461
Jørgensen, J. K., Schöier, F. L., & van Dishoeck, E. F. 2002, A&A, 389, 908
Kaufman, M. J., Wolfire, M. G., Hollenbach, D. J., & Luhman, M. L. 1999, ApJ, 527, 795
Kessler, M. F., Steinz, J. A., Anderegg, M. E., et al. 1996, A&A, 315, L27
Knee, L. B. G., & Sandell, G. 2000, A&A, 361, 671
Langer, W. D., Castets, A., & Lefloch, B. 1996, ApJ, 471, L111
Lay, O. P., Carlstrom, J. E., & Hills, R. E. 1995, ApJ, 452, L73
Lee, H.-H., Bettens, R. P. A., & Herbst, E. 1996, A&AS, 119, 111
Lefloch, B., Castets, A., Cernicharo, J., Langer, W. D., & Zylka, R. 1998, A&A, 334, 269
Lis, D. C., Keene, J., Phillips, T. G., et al. 2001, ApJ, 561, 823
Liseau, R., Ceccarelli, C., Larsson, B., et al. 1996, A&A, 315, L181
Looney, L. W., Mundy, L. G., & Welch, W. J. 2000, ApJ, 529, 477
Melnick, G. J., Stauffer, J. R., Ashby, M. L. N., et al. 2000, ApJ, 539, L77
Molinari, S., Ceccarelli, C., White, G. J., et al. 1999, ApJ, 521, L71
Molinari, S., Noriega-Crespo, A., Ceccarelli, C., et al. 2000, ApJ, 538, 698
Moneti, A., Cernicharo, J., & Pardo, J. R. 2001, ApJ, 549, L203

Motte, F., & André, P. 2001, A&A, 365, 440
Neufeld, D. A., Snell, R. L., Ashby, M. L. N., et al. 2000, ApJ, 539, L107
Nisini, B., Benedettini, M., Giannini, T., et al. 1999, A&A, 350, 529
Poglitsch, A., Herrmann, F., Genzel, R., et al. 1996, ApJ, 462, L43
Sandell, G., & Knee, L. B. G. 2001, ApJ, 546, L49
Sandell, G., Aspin, C., Duncan, W. D., Russell, A. P. G., & Robson, E. I. 1991, ApJ, 376, L17
Schöier, F. L., Jørgensen, J. K., van Dishoeck, E. F., & Blake, G. A. 2002, A&A, 390, 1001
Schilke, P., Walmsley, C. M., Pineau des Forets, G., & Flower, D. R. 1997, A&A, 321, 293
Shu, F. H. 1977, ApJ, 214, 488
Swinyard, B. M., Burgdorf, M. J., Clegg, P. E., et al. 1998, in Infrared Astronomical Instrumentation, ed. M. Fowler Albert, Proc. SPIE 3354, 888
Takahashi, T., Silk, J., & Hollenbach, D. J. 1983, ApJ, 275, 145
Tielens, A. G. G. M., Tokunaga, A. T., Geballe, T. R., & Baas, F. 1991, ApJ, 381, 181
van Dishoeck, E. F., Blake, G. A., Jansen, D. J., & Groesbeck, T. D. 1995, ApJ, 447, 760
Vastel, C., Caux, E., Ceccarelli, C., et al. 2000, A&A, 357, 994
Walmsley, C. 1989, in Interstellar Dust, IAU Symp., 135, 263